Geochemistry Geophysics Geosystems G3

Published by AGU and the Geochemical Society

Article
Volume 14, Number 4
24 April 2013
doi:10.1002/ggge.20076
ISSN: 1525-2027

Laboratory observation of acoustic fluidization in granular fault gouge and implications for dynamic weakening of earthquake faults

Kaiwen Xia
State Key Laboratory of Hydraulic Engineering Simulation and Safety, School of Civil Engineering, Tianjin University, Tianjin, China

Department of Civil Engineering, University of Toronto, Toronto, Ontario, Canada

Sheng Huang
Department of Civil Engineering, University of Toronto, Toronto, Ontario, Canada

Chris Marone
Department of Geosciences, Pennsylvania State University, University Park, Pennsylvania, USA (cjm38@psu.edu)

[1] Several lines of evidence, including remote triggering of earthquakes and modulation of seismic tremor by Earth tides, suggest that faults weaken when subject to shaking and dynamic stresses associated with the passage of seismic waves. However, the origin of such dynamic weakening is poorly understood. Here we explore the role of acoustic resonance for dynamic fault weakening using laboratory measurements. Experiments were conducted using a split Hopkinson pressure bar assembly, with dynamic stressing via impact loading. Samples were composed of crushed rock particles from mine tailings with a particle size distribution similar to that found in a natural fault gouge. We used pulse-shaper techniques and carefully evaluated dynamic stresses recorded at the front and rear of the sample to ensure that dynamic force balance was satisfied. Our experiments document acoustic-induced fluidization and dramatic dynamic weakening. Frictional strength and elastic modulus of a simulated fault gouge are reduced by a factor of 5–10 via acoustic fluidization. We find a threshold acoustic pressure for fluidization that varies systematically with gouge zone properties. Our observations could help explain dynamic fault weakening and triggering of earthquake fault slip by dynamic stressing.

Components: 6,500 words, 9 figures.

Keywords: Earthquakes; acoustic; fluidization; granular; tectonic fault.

Index Terms: 5102 Fracture and flow.

Received 6 December 2012; **Accepted** 29 January 2013; **Published** 24 April 2013.

Xia K., S. Huang, and C. Marone (2013), Laboratory observation of acoustic fluidization in a granular fault gouge and implications for dynamic weakening of earthquake faults, *Geochem. Geophys. Geosyst.*, *14*, 1012–1022, doi:10.1002/ggge.20076.

1. Introduction

[2] Earthquakes are often triggered by relatively small changes in stress [*Hill et al.*, 1993; *Stein*, 1999; *Kilb et al.*, 2000; *Gomberg et al.*, 2004; *Gomberg and Johnson*, 2005; *Freed*, 2005; *Rubinstein et al.*, 2008; *Gomberg*, 2010; *Pollitz et al.*, 2012; *Gonzalez-Huizar et al.*, 2012], which suggests that faults weaken when subject to shaking. Recent studies have indicated that a wide spectrum of fault

slip behaviors, including slow earthquakes and seismic fault tremor, may be also triggered by dynamic stressing [*Felzer and Brodsky*, 2006; *Rubinstein et al*., 2007, 2008; *Gomberg et al*., 2008; *Miyazawa and Brodsky*, 2008; *Hawthorne and Rubin*, 2010; *Peng and Gomberg*, 2010; *Peng et al*., 2010; *Itaba and Ando*, 2011; *Shelly et al*., 2011; *Ader et al*., 2012; *Thomas et al*., 2012; *Johnson et al*., 2012]. Existing laboratory studies show that frictional slip can be initiated by transient loading [*Boettcher and Marone*, 2004; *Johnson et al*., 2008; *Savage and Marone*, 2008]; however, understanding the mechanisms of fault weakening by dynamic stresses is limited by our knowledge of dynamic weakening mechanisms for frictional tectonic fault zones.

[3] Fault weakening under conditions of dynamic earthquake rupture has been attributed to several factors, including thermal pressurization, hydrodynamic effects, extreme frictional weakening at high slip velocity, and changes in damage zone permeability [e.g., *Brodsky and Kanamori*, 2001; *Perfettini et al*., 2001; *Johnson and Jia*, 2005; *Wibberley and Shimamoto*, 2005; *Di Toro et al*., 2006; *Ampuero and Ben-Zion*, 2008; *Johnson et al*., 2008; *Noda et al*., 2009; *Di Toro et al*., 2011; *Duan et al.*, 2011; *Mitchell and Faulkner*, 2012]. Modulus softening via nonlinear elastic effects and frictional melting during seismic slip have been proposed as fault-weakening mechanisms based on laboratory and field studies [e.g., *Johnson and Jia*, 2005; *Di Toro et al*., *2006*, *2011*; *Brunet et al*., 2008a, 2008b]; however, existing laboratory studies of dynamic stressing of a fault gouge have explored primarily low amplitude and/or long period modulations of shear strength. These studies show reduction of frictional strength during steady state sliding [*Boettcher and Marone*, 2004], triggering and disruption of stick-slip recurrence [*Johnson et al*., 2008; *Savage and Marone*, 2008], and modulus reduction for confined granular materials [*Brunet et al*., 2008a, 2008b]. However, the effects are generally small and may require specialized conditions to operate.

[4] Acoustic fluidization is another form of dynamic fault weakening, and relatively little laboratory work has been done to investigate this mechanism. Melosh [1979, 1996] proposed that acoustic fluidization could occur if dynamic stresses associated with seismic waves produce elastodynamic resonance as they propagate within or through a fault zone. He postulated that elastic strain energy could excite strong, short-wavelength vibrations in the fault core and that the resulting stress fluctuations could generate an acoustic pressure that was sufficient to temporarily reduce effective normal stress (but see *Sornette and Sornette*, 2000).

[5] Acoustic fluidization is attractive as a dynamic fault-weakening mechanism because it operates independently of, and potentially in concert with, other fault-weakening mechanisms [*Collins and Melosh*, 2003]. However, only a few laboratory measurements exist that could be used to test the theory of acoustic fluidization in tectonic fault zones [e.g., *Brunet et al*., 2008a, 2008b; *van der Elst et al*., 2012], and existing data address stress conditions that are much lower than those expected for seismogenic faults.

[6] The purpose of this paper is to report our laboratory investigations of acoustic fluidization in a simulated fault gouge under seismogenic stresses. We conducted laboratory experiments on granular materials used to simulate wear material (gouge) in earthquake fault zones. Samples were subjected to acoustic excitation via compressive stress pulses generated by high-speed impact. We find significant reduction of the frictional flow stress and elastic modulus of the granular gouge, consistent with acoustic fluidization.

1.1. Acoustic Fluidization

[7] Melosh [1979, 1996] proposed that dynamic stressing of a granular fault gouge at acoustic frequencies could generate internal stresses P that counteract the effective normal stress σ, leading to reduction of frictional strength (Figure 1). Granular fluidization is expected when the acoustic pressure is of the same order as the tectonic stresses at seismogenic depths (tens of megapascals).

[8] As applied to tectonic faulting, acoustic fluidization is described by the parameter $f = r\sum^2$, where $r = eQ/2$ and $\sum$ is the normalized shear stress on the fault ($\sum = \tau/\rho gh$). In these expressions, e is the fraction of mechanical work converted to seismic or acoustic waves and is typically ~0.1, Q is the quality factor of the material [*Knopoff*, 1964], and ρgh is the lithostatic stress due to overlying rock.

[9] According to theory [*Melosh*, 1979, 1996], fluidization may occur when f exceeds 2.8. The dependence of fluidization on acoustic vibration frequency is through Q, which is given by $Q = (2\pi l_g/\lambda)$ [*Knopoff*, 1964]. Here l_g is the absorption length and λ is the wavelength of the acoustic wave. The wavelength of the acoustic wave is related to the thickness of the fault zone (Figure 1)

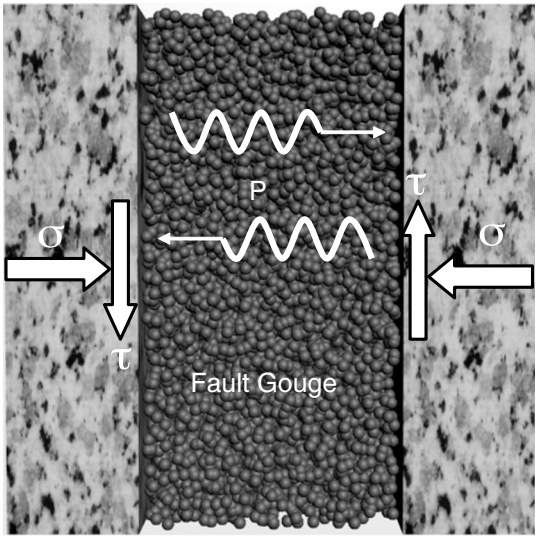

Figure 1. Idealized fault zone with the granular gouge showing application of acoustic fluidization to earthquake dynamics. Dynamic stresses associated with distant earthquakes, or rupture propagation along this fault, generate acoustic pressure P, which counteracts the fault normal stress σ, causing fluidization and frictional slip at low resolved shear stress τ.

through the phenomenon of resonance. Narrower zones require larger values of f, consistent with the requirement that the ratio of acoustic energy trapped within the fault zone to energy scattered outside the fault be maintained above a critical threshold. Granular acoustic fluidization is facilitated by short-wavelength (small λ) excitation, less attenuating granular media (large l_g), and large wave amplitude.

2. Experimental Methods

[10] Our experiments are designed to investigate the constitutive response of granular materials that constitute a fault gouge (Figure 1). We used finely crushed rock particles from mine tailings to simulate a granular fault gouge. The gouge is composed of quartz, feldspar, and minor amounts of barite and pyrite [*Klein and Simon*, 2006]. Granular samples were baked in a furnace at 100°C for 24 h and then crushed and sieved to obtain particles from 2 to 100 μm with a median effective diameter of 25 μm. The resulting particle size distribution is similar to that found in a natural fault gouge (Figure 2).

[11] To simulate the natural setting of fault gouges (Figure 1), granular particles were deformed as thin layers. Samples were constructed by loading particles into a plastic sample tube holder and then

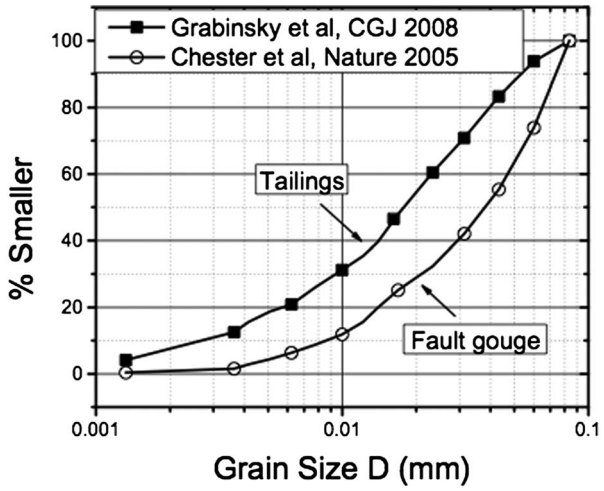

Figure 2. The particle size distribution of the simulated fault gouge used in this study (tailings) is similar to that of the natural fault gouge.

sealing the tube for dynamic impact. The sample holder is made of polycarbonate and has an inner and outer diameter of 25 and 37.5 mm, respectively (Figure 3). The bulk density of the sample is 1800 kg/m^3, equivalent to a solid volume fraction of 0.66.

[12] The sample assembly was loaded dynamically by a 25 mm diameter split Hopkinson pressure bar (SHPB) [*Kolsky*, 1953]. In our configuration, a loading stress pulse is induced by impact of a short striker bar (200 mm) on the input bar (1600 mm). All bars are made of 7075 aluminum alloy. Stresses are transmitted to the sample (Figure 3) via the input bar, and we record the complete dynamic stressing history using strain gauges on the input and output bars. Note that the stress waves shown in Figure 3 are schematic. As described below, we

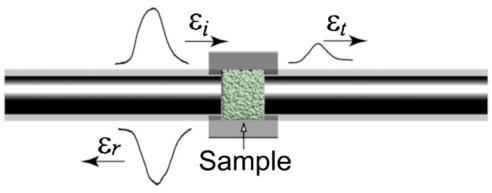

Figure 3. Schematic of the sample assembly for dynamic testing of granular materials. The granular sample (green) is held between rigid pistons (black) in the split Hopkinson pressure bar apparatus during dynamic impact. We record the stress wave incident on the sample (ε_i) and both the reflected (ε_i), and transmitted (ε_t) waves. The loading rate and the sample response are measured on each end of the assembly to ensure dynamic stress equilibration.

use pulse-shaper techniques, and thus, the wavelengths of stress pulses are longer than our granular samples.

[13] We measured the incident (ε_i), reflected (ε_r), and transmitted (ε_t) waves to obtain the stress history on the front and back surfaces of the sample (Figure 3). Data are recorded at 10 MHz and 12 bit digital resolution. The stress state in the sample is essentially one-dimensional strain due to the large difference in modulus between the sample and the holder.

[14] Based on the one-dimensional stress theory, we determine the histories of strain rate $\dot{\varepsilon}_i(t)$, strain $\varepsilon(t)$, and stress $\sigma(t)$ within the sample as [*Kolsky et al.*, 1949]

$$\begin{cases} \varepsilon(t) = \dfrac{C}{L}(\varepsilon_i + \varepsilon_r + \varepsilon_t) \\ \varepsilon(t) = \dfrac{C}{L}\displaystyle\int_o^t (\varepsilon_i + \varepsilon_r + \varepsilon_t) \\ \sigma(t) = \dfrac{A_b}{2A} E(\varepsilon_i + \varepsilon_r + \varepsilon_t) \end{cases} \quad (1)$$

where C is the one-dimensional longitudinal stress wave velocity of the bar, E is the Young's modulus of the bar, A_b is the cross-sectional area of the bar, L is the thickness of the simulated gauge sample, and A is the cross-sectional area of the sample. The bar material in our apparatus is 7075 aluminum alloy: density 2810 kg/m^3, Young's modulus 71.7 GPa, and Poisson's ratio 0.33. Assuming that stress equilibrium prevails during dynamic loading (i.e., $\varepsilon_i + \varepsilon_r = \varepsilon_t$), and noting that in our configuration, $A_b = A$, equation (1) can be simplified to

$$\begin{cases} \dot{\varepsilon}(t) = -\dfrac{2C}{L}\varepsilon_r \\ \varepsilon(t) = -\dfrac{2C}{L}\displaystyle\int_0^t \varepsilon_r dt \\ \sigma(t) = E\varepsilon_t \end{cases} . \quad (2)$$

[15] We note that the stress equilibrium condition is a prerequisite for constitutive tests of materials using the SHPB [*Kolsky et al.*, 1949].

2.1. Verification of Dynamic Stress Equilibrium

[16] We used pulse-shaper techniques [*Frew et al.*, 2001; *Xia et al.*, 2008] to achieve stress equilibrium and to ensure that dynamic force balance was satisfied for all of our tests (i.e., $\varepsilon_i + \varepsilon_r = \varepsilon$). This approach involves careful evaluation and modification of the dynamic stresses on each side of the sample (Figure 3), and we assume negligible energy loss due to heat and deformation, consistent with previous studies [e.g., *Xia et al.*, 2008]. For SHPB tests, the pulse-shaper technique involves modifying ("shaping") the input stress pulse using a small disc attached at the impact end of the incident bar. During the impact, the striker bar hits the shaper first, and because the shaper is made of a softer material than the bar (typical shaper discs are made of rubber or copper), the impact causes plastic deformation of the shaper, which results in increased risetime and extended duration of the stress pulse incident on the sample. Pulse-shaper techniques are designed to ensure stress equilibrium by extending the duration of the stress pulse applied to the sample. Because it takes time for the wave to transverse the sample, thicker samples require longer time to reach an equilibrium stress state. In the current experiments, we found that stress equilibrium was possible only for samples less than 8 mm in thickness (Figure 3).

[17] Figure 4 shows details of the dynamic stress balance check for two typical experiments. Stress applied to the front surface of the sample is proportional to the sum of the incident (In) and reflected waves (Re). For each test, we verify dynamic stress equilibrium by comparing the measured transmitted waves with the sum of the incident and reflected waves (Figure 4). For all of our experiments, the measured transmitted stress history is well matched by the sum of the input and reflected stresses (Figure 4), which verifies dynamic stress equilibrium.

3. Results

[18] Figure 5 shows typical incident wave loading histories as a function of impact velocity for our experiments. We varied the impact velocity of the striker to generate different dynamic stress levels and stressing histories, such as expected for dynamic stresses from near and distant earthquakes. For impacts of 1–12 m/s, the maximum stresses and center frequencies of the imposed loading pulses are ~4–40 MPa and 2–3 kHz, respectively (Figure 5). Higher impact velocities are used to generate larger peak forces and higher stressing rates. For our samples, the peak impact forces range from 2 kN for impact velocities of 1 m/s to 20 kN for impacts at 12 m/s, with corresponding shifts in the loading rates and durations (Figure 5). Note that although we used the 200 mm striker bar for all tests, pulses with different durations are obtained because the pulse duration is a function of the plastic wave velocity and, thus, the plastic strain

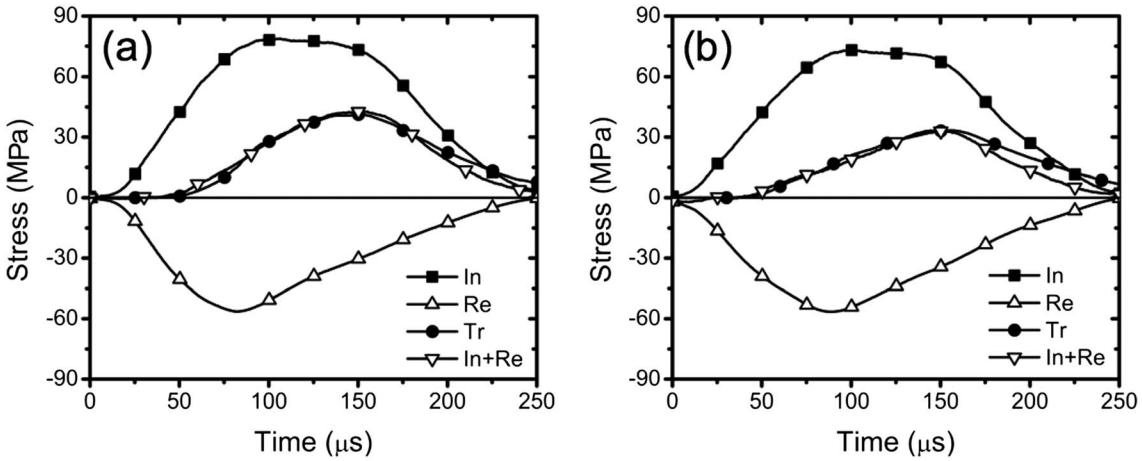

Figure 4. Detailed measurements of dynamic stressing in the SHPB system. The data sampling rate is 10 MHz, and symbols are only used to distinguish the curves. Stress applied to the front surface of the sample is proportional to the sum of the incident (In) and reflected waves (Re). Stress on the back surface of the sample is proportional to the transmitted wave (Tr). For each test, we perform a dynamic stress equilibrium test by comparing the measured incident, reflected, and transmitted waves. (a) Data for a 5 mm thick layer of gouge. (b) Data for an 8 mm thick layer. In each case, the transmitted wave is well matched by the sum of the incident and reflected waves, which indicates that dynamic stress equilibrium is achieved.

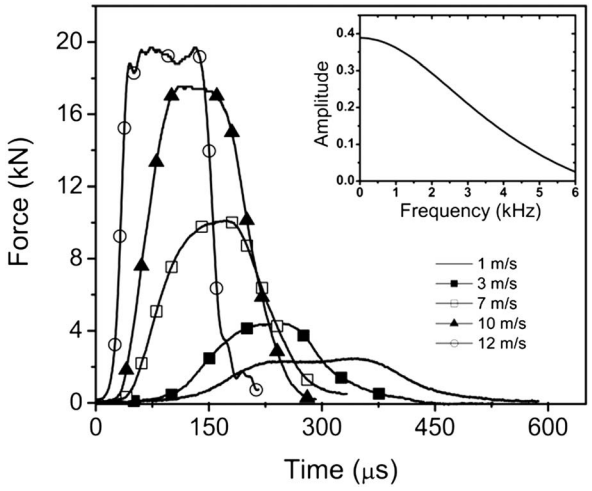

Figure 5. Typical incident wave loading history as a function of striker velocity (see legend). Note that peak applied force and duration increases with striker velocity. Inset shows the loading frequency spectrum for 10 m/s impact.

in the shaper, which, in turn, is a function of the impact stress and, thus, the impact velocity.

3.1. Two Types of Friction and Flow Responses

[19] Figure 6a shows the dynamic strength properties for three gouge thicknesses tested at impact velocities near 10 m/s. These stress-strain curves exhibit initial compaction for strains up to 0.5% followed by an increase in stress. Under identical loading conditions, 8 mm thick gouge layers behave quite differently than 3 and 5 mm thick gouges (Figure 6a). After compaction, the 8 mm layer exhibits a typical constitutive response for a granular solid, with a roughly linear increase in shear stress for strains >1%. In contrast, for the 3 and 5 mm layers, the elastic regime is negligible, and plastic flow at a low stress is observed almost immediately for strains >1% (Figure 6a).

[20] The stress-strain curves for 3 and 5 mm thick layers of the gouge (Figure 6a) are typical of fluids and soft materials such as rubber [*Song et al.*, 2007]. The 3 and 5 mm thick gouge samples fail by granular flow at low resolved shear stresses, suggesting a "fluid-like" response. In contrast, the 8 mm thick gouge layers show nearly 10 times the shear strength at 2% strain compared to that of the thinner layers, (Figure 6a). These results suggest a critical sample thickness for a transition from solid to fluidized behavior under the same dynamic stress conditions, which is consistent with Melosh's theory [*Melosh*, 1979, 1996].

3.2. Numerical Verification

[21] To verify that results such as those of Figure 6a are not an artifact of the loading configuration or testing apparatus, we used a finite element model to simulate the constitutive response for various

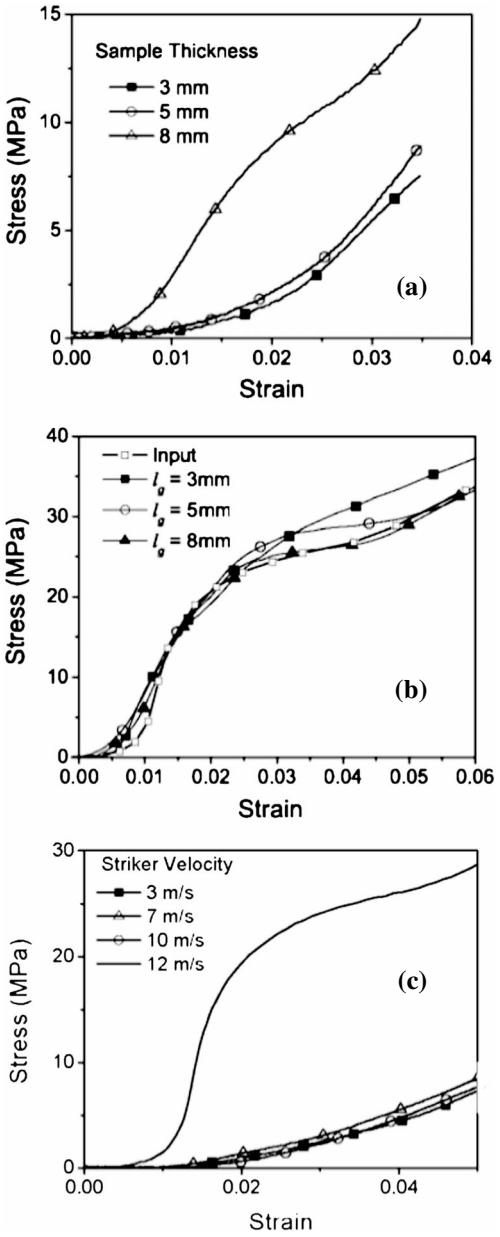

Figure 6. Dynamic strength and constitutive behavior of the simulated fault gouge. (a) Stress-strain curves derived from dynamic measurements on three layer thicknesses. Note that 3 and 5 mm thick layers exhibit fluid-like behavior characterized by large strain and slow stress increase, whereas the 8 mm thick layer is strong and typical of a granular solid. Impact velocity is 10 m/s in each case. (b) Numerical simulation results calculated for 12 m/s impact and different layer thicknesses. Note that solid response is observed in each case. (c) Effect of loading rate for 5 mm thick layers. Impact velocities below 12 m/s result in a fluid-like response.

sample thicknesses. Numerical simulations were done with LS DYNA [2001]. For the simulations, the stress-strain curve for a 12 m/s impact on a 5 mm thick layer was used as a tabulated material constitutive model, and the measured incident wave for this test was used as input. We note that LS DYNA allows one to use this form of constitutive model, tabulated values of stress and strain, without referring to explicit constitutive equations, and we used this approach for the simulations.

[22] Reflected and transmitted waves were computed and used to calculate the stress-strain curve of the material using equation (2). As shown in Figure 6b, the results of our numerical tests predict solid-like stress-strain behavior for our full range of conditions. This indicates that the dynamic weakening we observe for 3 and 5 mm thick layers (Figure 6a) is a material response and not an artifact of the experimental configuration.

3.3. Critical Impact Velocity and Loading Rate

[23] There are two variables in our experiments: gouge thickness and loading level via striker impact velocity. Figure 6c shows the stress-strain curves for 5 mm layers subject to a range of impact velocities. The constitutive response shows a dramatic change between 10 and 12 m/s. Lower impact velocities yield fluidized behavior, whereas the behavior for 12 m/s resembles a typical frictional solid.

[24] In our experiments, higher impact velocities cause higher peak stresses and higher rates of confinement stress increase (Figure 5). Thus, the data in Figure 6c are consistent with a transition from conditions that favor acoustic fluidization (when acoustic pressure P exceeds confining stress σ) below 12 m/s to those in which σ exceeds P. If this interpretation is correct, we expect that the critical impact velocity for dynamic weakening should vary with both layer thicknesses and consolidation state.

[25] We tested the interpretation that acoustic fluidization is hindered by consolidation state and confining stresses by using prestressed samples (Figure 7). These experiments used 5 mm thick samples that were precompacted via a prestress of ~2 MPa in the bar axial direction. To achieve the pretress, the front (impact) end of the incident bar is fixed, and the load is applied on the rear end of the transmitted bar using a hydraulic press.

[26] Prestressed samples were subjected to impact velocities from 8 to 11 m/s (Figure 7). For samples loaded by impact at 11 m/s, preconsolidation had a marked effect. The preconsolidated sample showed solid-like behavior, whereas the non prestressed sample showed fluid-like behavior (Figure 7),

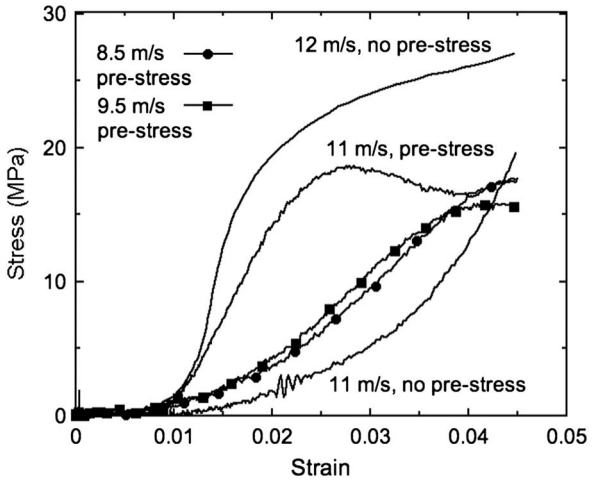

Figure 7. Constitutive behavior for 5 mm thick layers with and without prestressing at 2 MPa stress prior to impact. Note that the nonprestressed sample loaded at 11 m/s shows fluidized behavior, whereas the corresponding prestressed sample impacted at the same velocity shows behavior typical of a granular solid. Prestress enhances granular friction and inhibits acoustic fluidization.

consistent with our main results on the effect of stressing rate and impact velocity (Figure 6c). Preconsolidation also inhibited acoustic fluidization in samples loaded at lower impact velocity (Figure 7). Samples loaded at 8.5 and 9.5 m/s showed a tendency for solid frictional shear, in contrast to the behavior for similar impact velocities on nonprestressed samples, which flowed at low resolved shear stress (Figure 6c). We note that the prestress state in the sample, just like the dynamic stress state applied in a SHPB test, is approximately one-dimensional strain. This is a result of the large difference in rigidity between the polycarbonate and the simulated fault gouge. Thus, when the gouge flows, the stress state is, dynamically, hydrostatic. It would be useful and interesting to explore a wider range of preconsolidation states, given that in tectonic fault zones, one might expect different material properties, and therefore different acoustic responses, as a function of time during the seismic cycle; however, those tests are beyond the scope of the present study.

[27] These data are consistent with the idea that acoustic pressure exceeds confining pressure and induces fluidization for the lower impact velocities in our study. Our interpretation is that above a threshold impact velocity, the rate of confining stress increase exceeds the rate of acoustic stress increase, producing solid friction behavior (Figure 7). We posit that prestressed samples are more compacted, and thus, acoustically generated stresses must overcome a combination of granular friction, dynamic compressive stress, and static confining stresses to induce fluidization.

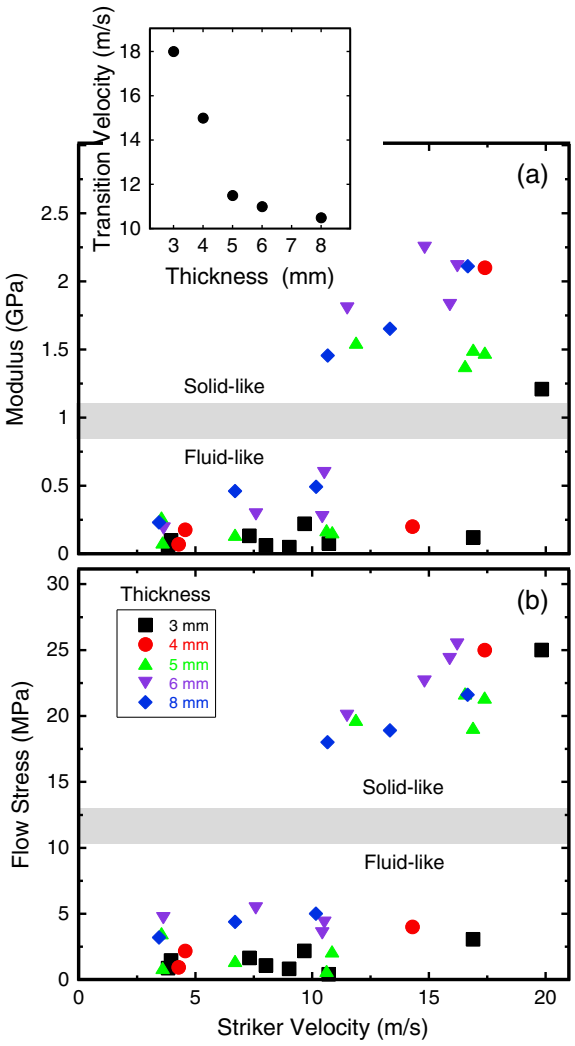

Figure 8. Elastic properties and dynamic strength as a function of striker velocity for five gouge layer thicknesses. (a) Modulus obtained via a linear fit of the stress-strain curve for strains from 1% to 2%. For a given layer thickness, modulus is low for striker velocities below a critical value and high, consistent with solid behavior, for higher velocities. (b) Flow stress at 2% strain. For a given layer thickness, fluidization occurs for velocities below a critical value. Note that larger impact velocities, and thus larger peak force, are required to fluidize thinner layers. Inset shows critical transition velocity for fluidization as a function of layer thickness.

3.4. A Phase Diagram for Acoustic Fluidization in Granular Fault Gouge

[28] We conducted dynamic loading experiments for a wide range of gouge layer thicknesses and impact velocities. Figure 8 shows elastic modulus and frictional flow strength as a function of striker

velocity for a range of gouge layer thicknesses. Elastic modulus is obtained by a linear fit of the stress-strain curve (e.g., Figure 6) for strains from 1% to 2%. Values of frictional strength correspond to the flow stress at a strain of 2%. Figure 8a shows two sets of moduli: one ≤0.6 GPa and the other ≥1.2 GPa. The lower values are consistent with fluidized behavior, while the higher values are consistent with behavior for a granular solid.

[29] For a given gouge layer thickness, we observe a clear transition from fluidized to solid behavior as a function of striker velocity (Figure 8a). The critical impact velocity for fluidization decreases systematically as a function of gouge thickness (inset in Figure 8), consistent with theory [*Melosh*, 1979, 1996]. We note that the differences in modulus for solid-like and fluidized behaviors are significantly larger than those reported in previous works on dynamic stressing [e.g., *Boettcher and Marone*, 2004; *Johnson and Jia*, 2005; *Johnson et al*., 2012; *van der Elst et al*., 2012].

[30] Measurements of frictional strength at 2% strain also exhibit two clusters (Figure 8b): one <6 MPa and another >18 MPa. We interpret the lower strength cluster as evidence of fluidized behavior and the high cluster as solid behavior. Because the stress applied to our sample scales with impact velocity, these data indicate that the critical fluidization stress is lower for thicker gouge layers, consistent with theory [*Melosh*, 1979, 1996].

4. Discussion

[31] Our data are broadly consistent with acoustic fluidization theory [*Melosh*, 1979, 1996]. We note in particular that the elapsed time during loading and the time expected for generation and dissipation of acoustic energy agree, as required by theory. Consistency between the theory and our experimental evidence also comes from the dependence of fluidization on the frequency of the acoustic wave. That is, thinner samples fluidize more readily because the acoustic waves excited are higher frequency. Also, the observation of lower frictional strength at lower striker velocity is consistent with lower acoustic energy, as noted in Melosh [1996]. Fluidization occurs when the acoustic pressure is higher than the sample confinement produced by the induced stress state. At low impact speed, the confinement due to dynamic loading is lower, while the frequency of the acoustic pressure induced by reverberation is essentially the same. As a result, lower impact velocity facilitates fluidization.

[32] In our experiments, both the effective confining pressure for the sample and the acoustic excitation are induced by the stress wave pulse. Higher speed impact causes higher compressive stresses and greater acoustic excitation. Fluidization requires that acoustic pressure exceed confinement stress. Thus, acoustic fluidization is expected to occur in an optimal range of stressing rate dictated by granular strength, the rate of acoustic pressure generation, and confinement.

[33] Our sample assembly shares features of natural fault zones, where the gouge is surrounded by more competent wall rock (Figure 1). The imposed loading pulse in experiments corresponds to incoming seismic waves from nearby earthquakes or, for a nonplanar fault, other sections of the same fault during dynamic rupture propagation. Depending on the propagation direction and mode of seismic wave, dynamic loading of the fault zone can be compressive, as in our experiments, or shear.

[34] During acoustic fluidization, the fault gouge amplifies the energy at high frequency via granular processes. The resulting acoustic pressure P may exceed the lithostatic and tectonic confining stresses, which would cause fluidization. This could occur via dynamic stressing of a quasi-statically stressed fault, for example, via the passage of seismic waves from another earthquake, or as a product of elastic radiation during dynamic rupture propagation. The latter case would correspond to dynamic fault weakening, whereas the former case would indicate dynamic earthquake triggering. In either case, acoustic waves may cause a dramatic reduction of shear strength, leading to earthquake instability, aseismic creep, or subcritical rupture growth. The latter behaviors could yield transiently accelerating creep and Earth tremor or earthquakes with enhanced low frequency content. A key point is that acoustic fluidization could cause immediate dynamic weakening or initiate an incubation period for delayed failure.

[35] The application of our data to tectonic faults is an important issue and one that is difficult to address directly. One approach is to compare the acoustic pressure inferred from our experiments with expected stress conditions at seismogenic depths. Based on the understanding that fluidization occurs when the acoustic pressure overcomes the confinement pressure, we can estimate the peak acoustic pressure from experiments close to the phase boundary between solid-like and fluidized behaviors (Figure 8). These values are quite reasonable given typical expectations for the strength of

tectonic faults. In experiments featuring fluidized response, the acoustic pressure is equal to the dynamic loading pressure, which can be calculated based on the recorded stress waves. Granular fluidization can occur when the acoustic pressure is of the same order as the tectonic stresses (tens of megapascals), and our laboratory estimates of the critical stress are in this range.

[36] Acoustic fluidization is tightly linked to loading frequency and resonance effects associated with fault zone dimensions. Thus, to apply our data to tectonic faults, we must address the question of how to scale from laboratory gouge zones, a few millimeters in width, to tectonic faults with gouge zones of meters to tens of meters in width. The maximum resonant frequency for a fault zone scales inversely with width.

[37] In our experiments, we derive the resonance frequency f_c from the wave speed c and layer thickness L: $f_c = c/(2L)$. Wave speed can be obtained as $c = (M/\rho)^{1/2}$, where M is modulus (Figure 4a) and ρ is density (1800 kg/m^3). We may take average values of M for fluidized and solid behavior as 0.25 and 1.75 GPa, respectively. Figure 9 shows the relation between maximum resonance frequency and gouge layer thickness for our experiments. Our observations of fluidization indicate acoustic resonance at frequencies ranging from ~20 to 60 kHz. These values are above the center frequencies of our applied loads (Figure 5), which is consistent with their origin from acoustic resonance via particle-particle frictional collision events [*Jaeger et al*., 1996].

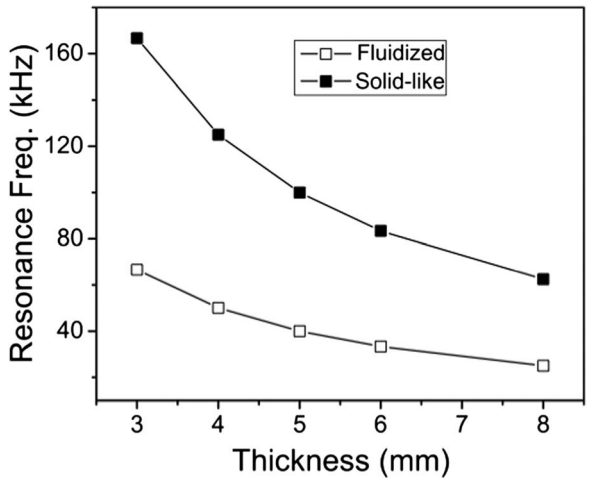

Figure 9. Maximum resonant frequency as a function of layer thickness for our tests. We use the average shear modulus and granular density to derive wave speed, which is ~1 km/s for solid behavior and ~0.4 km/s under fluidized conditions.

[38] For mature tectonic faults, the fault zone width is of order 1–10 m. Thus, we may speculate that this is the natural scale for acoustic resonance in fault zones. Using our measured shear wave speeds, these fault widths give resonant frequencies for acoustic fluidization of ~20 to 200 Hz, which is well within the seismic frequency range for a dynamically propagating rupture.

5. Conclusions

[39] Several lines of evidence show that earthquake faults weaken during dynamic rupture and upon dynamic stressing associated with the passage of seismic waves. Despite the richness of such observations, the mechanism of dynamic fault weakening remains poorly understood. Here we evaluate the role of acoustic fluidization as a mechanism of dynamic fault weakening and present laboratory experimental evidence documenting such weakening under seismogenic conditions. We test the interpretation that acoustic fluidization is hindered by confining stresses using preconsolidated samples. We find a threshold stressing rate for fluidization that scales systematically with gouge thickness.

[40] Our data indicate that dynamic stress waves may cause acoustic fluidization in tectonic fault zones and, consequently, reduction in elastic moduli and loss of frictional strength. These results are consistent with theory [*Melosh*, 1979, 1996], which indicates that dynamic weakening is driven by trapped acoustic energy that is magnified by resonance. In our experiments, acoustically generated pressure exceeds the confining pressure under some conditions. For a given gouge layer thickness, we observe a clear transition from fluidized to solid behavior as a function of striker velocity. Fluidization occurs at a critical impact velocity for a given layer thickness.

Acknowledgments

[41] Funding was provided by the Innovative Research Groups of the National Natural Science Foundation of China (NSFC) under Grant 51021004 and the Cooperation Project of NSFC under Grant 51228902 (K.X.), and by the U.S. National Science Foundation (C.M). K.X.'s research was partially supported by the National Basic Research Program of China (973 Program) under Grant 2013CB035904. We gratefully acknowledge critical review comments by H. J. Melosh and P. A. Johnson.

References

LS-DYNA User's Manual (2001), Livermore Software Technology Corporation, Livermore, CA.

Ader, T. J., J. P. Ampuero, and J. P. Avouac (2012), The role of velocity-neutral creep on the modulation of tectonic tremor activity by periodic loading, *Geophys. Res. Lett.*, *39*, L16310.

Ampuero, J. P., and Y. Ben-Zion (2008), Cracks, pulses and macroscopic asymmetry of dynamic rupture on a bimaterial interface with velocity-weakening friction, *Geophys. J. Int.*, *173*, 674–692.

Boettcher, M. S., and C. Marone (2004), Effects of normal stress variation on the strength and stability of creeping faults, *J. Geophys. Res.*, *109*, B03406.

Brodsky, E. E., and H. Kanamori (2001), Elastohydrodynamic lubrication of faults, *J. Geophys. Res.*, *106*, 16357–16374.

Brunet, T., X. Jia, and P. Mills (2008a), Mechanisms for acoustic absorption in dry and weakly wet granular media, *Phys. Rev. Lett.*, *101*, 138001.

Brunet, T., X. Jia, and P. A. Johnson (2008b), Transitional nonlinear elastic behaviour in dense granular media, *Geophys. Res. Lett.*, *35*, L19308.

Collins, G. S., and H. J. Melosh (2003), Acoustic fluidization and the extraordinary mobility of sturzstroms, *J. Geophys. Res.*, *108*(B10), 2473, doi:10.1029/2003JB002465.

Di Toro, G., et al. (2006), Natural and experimental evidence of melt lubrication of faults during earthquakes, *Science*, *311*, 647–649.

Di Toro, G., R. Han, T. Hirose, N. De Paola, S. Nielsen, K. Mizoguchi, F. Ferri, M. Cocco, and T. Shimamoto (2011), Fault lubrication during earthquakes, *Nature*, *471*, 494–498, doi:10.1038 /nature09.

Duan, B, K. Jingqian, and Y. G. Li (2011), Deformation of compliant fault zones induced by nearby earthquakes: Theoretical investigations in two dimensions, *J. Geophys. Res.*, *116*, , B03307, 10.1029/2010JB007826.

Felzer, K. R., and E. E. Brodsky (2006), Decay of aftershock density with distance indicates triggering by dynamic stress, *Nature*, *441*, 735–738.

Freed, A. M. (2005), Earthquake triggering by static, dynamic, and postseismic stress transfer, *Annu. Rev. Earth Planet. Sci.*, *33*, 335–367.

Frew, D. J., et al. (2001), A split Hopkinson pressure bar technique to determine compressive stress–strain data for rock materials, *Exp. Mech.*, *41*, 40–46.

Gomberg, J. (2010), Lessons from triggered tremor, *J. Geophys. Res.*, *115*, B10302, 10.1029/2009JB007011.

Gomberg, J., et al. (2004), Earthquake nucleation by transient deformations caused by the M = 7.9 Denali, Alaska, earthquake, *Nature*, *427*, 621–624.

Gomberg, J., and P. Johnson (2005), Dynamic triggering of earthquakes, *Nature*, *437*, 830.

Gomberg, J., et al. (2008), Widespread triggering of nonvolcanic tremor in California, *Science*, *319*, 173.

Gonzalez-Huizar, H., Velasco, A. A., Z. Peng, and R.R. Castro (2012), Remote triggered seismicity caused by the 2011 M9.0 Tohoku-Oki, Japan earthquake, *Geophys. Res. Lett.*, *39*, L10302.

Hawthorne, J. C., and A. M. Rubin (2010), Tidal modulation of slow slip in Cascadia, *J. Geophys. Res.*, *115*, B09406, 10.1029/2010JB007502

Hill, D. P., et al. (1993), Seismicity remotely triggered by the magnitude 7.3 Landers, California, earthquake, *Science*, *260*, 1617–1623.

Itaba, S., and R. Ando (2011), A slow slip event triggered by teleseismic surface waves, *Geophys. Res. Lett.*, *38*, L21306, 10.1029/2011GL049593.

Jaeger, H. M., et al. (1996), Granular solids, liquids, and gases, *Rev. Mod. Phys.*, *68*, 1259–1273.

Johnson, P. A., and X. Jia (2005), Nonlinear dynamics, granular media and dynamic earthquake triggering, *Nature*, *437*, 871–874.

Johnson, P. A., et al. (2008), Effects of acoustic waves on stick–slip in granular media and implications for earthquakes, *Nature*, *451*, 57–60.

Johnson, P., Carpenter, B. M., Knuth, M., Kaproth, B. M., Le Bas, P.-Y., Daub, E. G., and C. Marone (2012), Nonlinear dynamical triggering of slow slip on simulated earthquake faults with implications to Earth, *J. Geophys. Res.*, 10.1029/2011JB008594.

Kilb, D., et al. (2000), Triggering of earthquake aftershocks by dynamic stresses, *Nature*, *408*, 570–574.

Klein, K., and D. Simon (2006), Effect of specimen composition on the strength development in cemented paste backfill, *Can. Geotech. J.*, *43*, 310–324.

Knopoff, L. (1964), Q, *Rev. Geophys.*, *2*, 625–660.

Kolsky, H. (1953), *Stress Waves in Solids*, 212 pp., Clarendon Press, Oxford.

Kolsky, H., et al. (1949), An investigation of the mechanical properties of materials at very high rates of loading, *Proc. Royal Soc.*, *B62*, 676–700.

Melosh, H. J. (1979), Acoustic fluidization - new geologic process, *J. Geophys. Res.*, *84*, 7513–7520.

Melosh, H. J. (1996), Dynamical weakening of faults by acoustic fluidization, *Nature*, *379*, 601–606.

Mitchell, T. M., and D. R. Faulkner (2012), Towards quantifying the matrix permeability of fault damage zones in low porosity rock, *Earth Plan. Sci. Letts.*, *339–340*, 10.1016/j.epsl.2012.05.014.

Miyazawa, M., and E. E. Brodsky (2008), Deep low-frequency tremor that correlates with passing surface waves, *J. Geophys. Res.*, *113*, B01307.

Noda, H., et al. (2009), Earthquake ruptures with thermal weakening and the operation of major faults at low overall stress levels, *J. Geophys. Res.*, *114*, 1–27.

Peng, Z., and J. Gomberg (2010), An integrated perspective of the continuum between earthquakes and slow-slip phenomena, *Nature Geosci. 3*, 599–607.

Peng, Z., Hill, D. P., Shelly, D. R., and C. Aiken (2010), Remotely triggered microearthquakes and tremor in central California following the 2010 M[w] 8.8 Chile earthquake, *Geophys. Res. Lett.*, *37*, L24312, 10.1029/2010GL045462.

Perfettini, H., et al. (2001), Frictional response induced by time-dependent fluctuations of the normal loading, *J. Geophys. Res.*, *106*, 13455–13472.

Pollitz, F. F., R. S. Stein, V. Sevilgen, and R. Burgmann (2012), The 11 April 2012 east Indian Ocean earthquake triggered large aftershocks worldwide, *Nature*, *490*, 250–253.

Rubinstein, J. L., et al. (2007), Non-volcanic tremor driven by large transient shear stresses, *Nature*, *448*, 579–582.

Rubinstein, J. L., et al. (2008), Tidal modulation of nonvolcanic tremor, *Science*, *319*, 186–189.

Savage, H. M., and C. Marone (2008), Potential for earthquake triggering from transient deformations, *J. Geophys. Res.*, *113*, B05302.

Shelly, D. R., Z. Peng, D. P. Hill, and C. Aiken (2011), Triggered creep as a possible mechanism for delayed dynamic triggering of tremor and earthquakes, *Nature Geosci. 4*, 384–388.

Song, B., et al. (2007), Dynamic and quasi-static compressive response of porcine muscle, *J. Biomech.*, *40*, 2999–3005.

Sornette, D., and A. Sornette (2000), Acoustic fluidization for earthquakes, *Bull. Seis. Soc. Am.*, *90*, 781–785.

Stein, R. S. (1999), The role of stress transfer in earthquake occurrence, *Nature*, *402*, 605–609.

Thomas, A. M., Bürgmann, R., Shelly, D. R., Beeler, N. M., and M. L. Rudolph (2012), Tidal triggering of low frequency earthquakes near Parkfield, California: Implications for fault mechanics within the brittle-ductile transition, *J. Geophys. Res.*, *117*, B05301.

van der Elst, N. J., E. E. Brodsky, P.-Y. Le Bas, and P. A. Johnson (2012), Auto-acoustic compaction in steady shear flows: Experimental evidence for suppression of shear dilatancy by internal acoustic vibration, *J. Geophys. Res.*, *117*, B09314.

Wibberley, C. A. J., and T. Shimamoto (2005), Earthquake slip weakening and asperities explained by thermal pressurization, *Nature*, *436*, 689–692.

Xia, K., et al. (2008), Effects of microstructures on dynamic compression of Barre granite, *Int. J. Rock Mech. Mining Sci.*, *45*, 879–887.